

## Optical properties and photocatalytic activity of nanocrystalline TiO<sub>2</sub> doped by 3d-metal ions

I. V. Kolesnik<sup>1,2</sup>, V. A. Lebedev<sup>1</sup>, A. V. Garshev<sup>1,3</sup>

<sup>1</sup>Lomonosov Moscow State University, Leninskie Hills, 1, Moscow, 119992, Russia

<sup>2</sup>Institute of General and Inorganic Chemistry, Leninsky avenue, 31, Moscow, 119991, Russia

<sup>3</sup>Institute of Metallurgy, Leninsky avenue, 49, Moscow, 119334, Russia

kolesnik.iv@gmail.com, vasya\_lebedev@mail.ru, garshev@inorg.chem.msu.ru

PACS 61.46.+w, 61.46.-w, 71.55.-I, 78.20.-e, 78.40.Fy, 81.05.-t, 81.07.Bc, 82.50.Hp

DOI 10.17586/2220-8054-2018-9-3-401-409

The influence of impurities on optical and photocatalytic properties was studied in a series of nanocrystalline TiO<sub>2</sub> with similar coherent scattering region sizes, phase compositions, surface areas and lattice parameters doped by Fe, Cr, Mn and V ions. Doping leads to an increase of absorption in the visible part of the spectrum due to the formation of additional levels in the band gap. In the case of Fe and Cr ions, d-d transitions are observed, whereas in the case of Mn and V ions, an additional band is associated with the transition from impurity level to  $E_c$ . The presence of impurities effectively suppresses photocatalytic activity in the methyl orange decoloration reaction.

**Keywords:** titanium oxide, nanocrystalline, doped TiO<sub>2</sub>, photocatalysis, band gap, Urbach tail, impurity levels.

*Received: 11 November 2017*

### 1. Introduction

Tuning of photocatalytic properties of titanium dioxide is important for many practical applications of this material. One of the approaches to modify the photocatalytic activity of TiO<sub>2</sub> is doping by metal and non-metal ions. Different dopants such as metal ions: iron, chromium, nickel, manganese, niobium, cerium and other lanthanides, and non-metal atoms have been studied in detail [1–15].

In the case of TiO<sub>2</sub> doped with metal ions, which substitute Ti<sup>4+</sup>, or non-metals which substitute O<sup>2-</sup> or sit in interstitial positions the material absorbs light with higher wavelengths in comparison with undoped TiO<sub>2</sub>. Some authors associate this observation with the change of the band gap [16, 17]. Other authors suggest that the change of optical properties can be explained by the formation of additional energy levels in the band gap [18–20]. Such levels not only change optical properties but also may exert influence on the dynamics of the charge carriers.

For instance, it was observed [1, 14] that doping in titanium positions in TiO<sub>2</sub> lattice leads to the suppression of photocatalytic activity of TiO<sub>2</sub> because of the formation of defects such as oxygen vacancies, which may trap the electrons and form color centers. It is obvious that the type and concentration of defects partially determine photocatalytic activity of TiO<sub>2</sub> and should lead to the decrease of photocatalytic activity because of recombination processes. However many other works mentioned above demonstrate that doping leads to the increase of photocatalytic activity.

One can explain these contradictory tendencies by the influence of other factors which influence on photocatalytic activity of TiO<sub>2</sub>: crystallinity, particle size, phase composition and surface [21–23]. Introduction of impurity with subsequent calcinations at relatively high temperature lead to the situation when several characteristics within the same series of the samples change. For example, optical properties, grain size and crystallinity may change with the increase of dopant concentration because impurities influence on TiO<sub>2</sub> crystallization process.

In present study we used an approach which allowed us to distinguish the effects of the change of optical properties from microstructure and phase composition effects on the photocatalytic properties of metal doped TiO<sub>2</sub>. We prepared nanocrystalline TiO<sub>2</sub> with different concentrations of iron, chromium, vanadium and manganese impurities and with other characteristics such as phase composition, surface area, porosity and coherent scattering region sizes which were close to the parameters of non-doped samples. Their optical properties were studied by means of UV-Vis spectroscopy. The deconvolution of the spectra allowed us to find the positions of energy levels in the band gaps and to assign them to certain impurities, color centers and other processes. We also measured the photocatalytic properties of pure and doped nanocrystalline TiO<sub>2</sub> in the methyl orange decoloration reaction to find correlation between optical properties and photocatalytic activity.

## 2. Experimental

The synthesis of nanocrystalline  $\text{TiO}_2$  was performed by hydrolysis of  $\text{Ti}(\text{O}^i\text{C}_3\text{H}_7)_4$  (Aldrich, 97 %) in presence of triblock copolymer Pluronic (Aldrich, 95 %) in aqueous media. Titanium isopropoxide was added to the solution of the polymer,  $\text{NH}_4\text{F}$  (Sigma-Aldrich, 98 %) and  $\text{HNO}_3$  at pH=2 under vigorous stirring. The final composition of the reaction mixture was: 1  $\text{Ti}(\text{O}^i\text{C}_3\text{H}_7)_4$ : 0.016 P123 : 14.8  $\text{HNO}_3$  : 0.01  $\text{NH}_4\text{F}$  : 164  $\text{H}_2\text{O}$ . The suspension was stirred for 72 hours at room temperature; the precipitate was collected and washed several times by centrifugation. To prepare doped  $\text{TiO}_2$  proper amount of the corresponding salt ( $\text{Mn}(\text{NO}_3)_2 \cdot 4\text{H}_2\text{O}$  (Aldrich, 95 %),  $\text{Fe}(\text{NO}_3)_3 \cdot 9\text{H}_2\text{O}$  (Fluka, 95 %),  $\text{Cr}(\text{NO}_3)_3 \cdot 9\text{H}_2\text{O}$  (Sigma-Aldrich, 98 %),  $\text{NH}_4\text{VO}_3$  (Sigma-Aldrich, 99 %)) was added to the reaction mixture before the addition of  $\text{Ti}(\text{O}^i\text{C}_3\text{H}_7)_4$ . The following molar ratios of impurity to titanium were put into reaction mixtures: 0.05 %, 0.1 %, 0.5 %, 1 % and 3 %.

Characterization of pure and doped  $\text{TiO}_2$  was carried out by powder x-ray diffraction. X-ray diffraction patterns were acquired using a Rigaku D/MAX 2500 diffractometer equipped with  $\theta - 2\theta$  Bragg-Brentano reflection goniometer, Cu-rotating anode (40 kV, 250 mA), curved graphite monochromator placed at the reflected beam and a scintillation counter. Diffraction data were collected in the  $0.5 - 60 2\theta$  range with a 0.01 step and a fixation time of 2 s/step. The ICDD PDF-2 base was used to identify crystalline phases. The fitting of XRD profile was performed by means of Jana 2006 software [24]. Transmission electron microscopy (TEM) studies were performed at the Zeiss Libra 200 at 200 kV. Bright field TEM and selected area electron diffraction (SAED) images were collected using a CCD Gatan Ultrascan 4000 at  $2k \times 2k$  resolution. Adsorption and desorption isotherms of nitrogen were obtained at 77 K on a Quantachrome NOVA 4200e. The samples were outgassed at 473 K for 5 h before measurements were performed. The concentration of impurities was determined by mean of mass-spectrometry with inductively-coupled plasma (ICP MS) using ELAN DRC II Perkin Elmer spectrometer. Optical properties were analyzed by a UV-visible diffuse reflectance spectrometer Lambda 950 (Perkin Elmer) in the range 200 – 1100 nm.

Photocatalytic activity was measured by the decoloration of methyl orange in aqueous solution under UV illumination by high-pressure Hg bulb (5 W) in a cylindrical quartz IceGlass reactor with a thermostating contour.

## 3. Results and discussion

The concentrations of impurity ions in doped  $\text{TiO}_2$  samples were determined by ICP-MS (Table 1). One can see that molar ratio of impurity content to  $\text{TiO}_2$  is lower than in reaction mixture during the synthesis but systematically increases with increase of the concentration of metal salt in the reaction mixtures. The concentration of impurity changes had the following ranges: 0.03 to 1.63 mol. % for Fe-doped  $\text{TiO}_2$ ; 0.02 to 1.22 mol. % for Cr-doped  $\text{TiO}_2$ ; 0.03 to 1.44 mol. % for V-doped  $\text{TiO}_2$ ; 0.02 to 1.24 mol. % for Mn-doped  $\text{TiO}_2$ .

The structure and phase composition of pure and doped titanium oxide samples were characterized by low temperature nitrogen sorption, powder X-Ray diffraction and transmission electron microscopy. The parameters of the porous and crystalline structure as well as phase composition for all samples are similar (Table 1). All samples have high specific surface area (230 – 290  $\text{m}^2/\text{g}$ ) and consist of the mixture of anatase (80 – 90 %) and brookite (10 – 20 %) with the sizes of coherent scattering regions ranging from 4 – 6 nm. The formation of anatase phase during hydrolysis and relatively low temperature treatment is in good agreement with literature data [25]. Any other phases containing iron, chromium, vanadium and manganese have not been detected by X-Ray diffraction. The unit cell parameters were determined for anatase phase ( $a = 3.78 \pm 0.02 \text{ \AA}$ ,  $c = 9.48 \pm 0.09 \text{ \AA}$ ) and seem to be the same for all samples in the range of calculation uncertainty (Table 1) unlike Nb-doped samples in the same concentration range [26].

Typical TEM image of Cr-doped sample is presented on Fig. 1. The sample consists of the primary particles with diameters in the range 4 – 6 nm. This result is in good agreement with the result of calculation of coherent scattering region size for this sample. The other samples have the same microstructure according TRM data.

The electron diffraction pattern consists of concentric circles which are typical for polycrystalline samples. The values of  $d$  correspond to the anatase phase. The reflections for brookite phase are not clearly seen because of low brookite content, small particle size and because the most of the reflections of brookite phase overlap with the reflections of anatase.

Optical properties of pure and doped titanium oxide were studied by diffuse reflectance UV-Vis spectroscopy. The spectra are presented on the Fig. 2. All doped samples demonstrate the increase of absorption in visible region in comparison with pure  $\text{TiO}_2$ . Also, the intensity of visible light absorption increases with the increase of dopant concentration. The intensity of optical absorption depends not only on the concentration but also on the nature of the dopant. In the case of Fe- and Mn-doped  $\text{TiO}_2$ , we observe a shoulder near the absorption edge. Whereas in

TABLE 1. Impurity concentrations, specific surface areas, CSR sizes and unit cell parameters of anatase phases for pure and doped nanocrystalline TiO<sub>2</sub>

Impurity to titanium ratios ion reaction mixture (mol. %)	Impurity concentration (mol. %) determined by ICP MS	Specific surface area (m <sup>2</sup> /g)	CSR size (nm) and phase content (%)			Unit cell parameters of anatase, Å	
			anatase	5	90	a	3.78±0.02
Pure TiO <sub>2</sub>	–	270	brookite	6	10	c	9.48±0.09
			anatase	6	90	a	3.79±0.02
0.05 (Fe)	0.03	250	brookite	4	10	c	9.49±0.04
			anatase	6	90	a	3.80±0.01
0.1 (Fe)	0.09	240	brookite	4	10	c	9.51±0.06
			anatase	6	90	a	3.80±0.04
0.5 (Fe)	0.25	230	brookite	5	10	c	9.48±0.09
			anatase	6	90	a	3.79±0.02
1 (Fe)	0.53	270	brookite	4	10	c	9.53±0.07
			anatase	5	90	a	3.78±0.02
3 (Fe)	1.63	250	brookite	4	10	c	9.49±0.07
			anatase	5	90	a	3.81±0.02
0.05 (Cr)	0.02	230	brookite	4	10	c	9.53±0.06
			anatase	5	90	a	3.80±0.02
0.1 (Cr)	0.05	230	brookite	4	10	c	9.49±0.07
			anatase	5	90	a	3.81±0.03
0.5 (Cr)	0.24	230	brookite	5	10	c	9.48±0.07
			anatase	6	90	a	3.78±0.02
1 (Cr)	0.50	270	brookite	5	10	c	9.45±0.05
			anatase	5	90	a	3.90±0.01
3 (Cr)	1.22	250	brookite	4	10	c	9.49±0.02
			anatase	5	90	a	3.80±0.02
0.05 (Mn)	0.03	270	brookite	5	10	c	9.51±0.06
			anatase	6	80	a	3.80±0.02
0.1 (Mn)	0.07	290	brookite	5	20	c	9.50±0.06
			anatase	4	80	a	3.81±0.03
0.5 (Mn)	0.27	260	brookite	5	20	c	9.52±0.05
			anatase	5	90	a	3.78±0.02
1 (Mn)	0.35	290	brookite	5	10	c	9.49±0.05
			anatase	5	90	a	3.80±0.03
3 (Mn)	1.44	280	brookite	4	10	c	9.50±0.03
			anatase	5	90	a	3.81±0.01
0.05 (V)	0.02	260	brookite	5	10	c	9.52±0.08
			anatase	5	90	a	3.80±0.01
0.1 (V)	0.03	250	brookite	5	10	c	9.47±0.05
			anatase	5	90	a	3.81±0.02
0.5 (V)	0.18	280	brookite	4	10	c	9.50±0.05
			anatase	5	80	a	3.79±0.01
1 (V)	0.36	280	brookite	5	20	c	9.46±0.07
			anatase	5	80	a	3.81±0.02
3 (V)	1.24	250	brookite	4	20	c	9.49±0.04

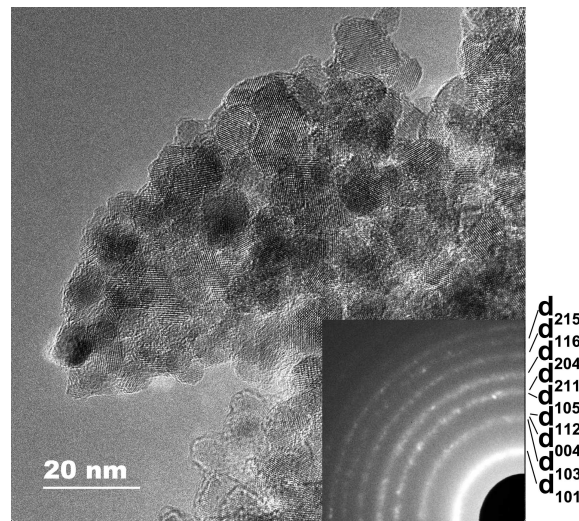


FIG. 1. Typical TEM image of Cr-doped nanocrystalline  $\text{TiO}_2$  (1.22 mol.% of Cr)

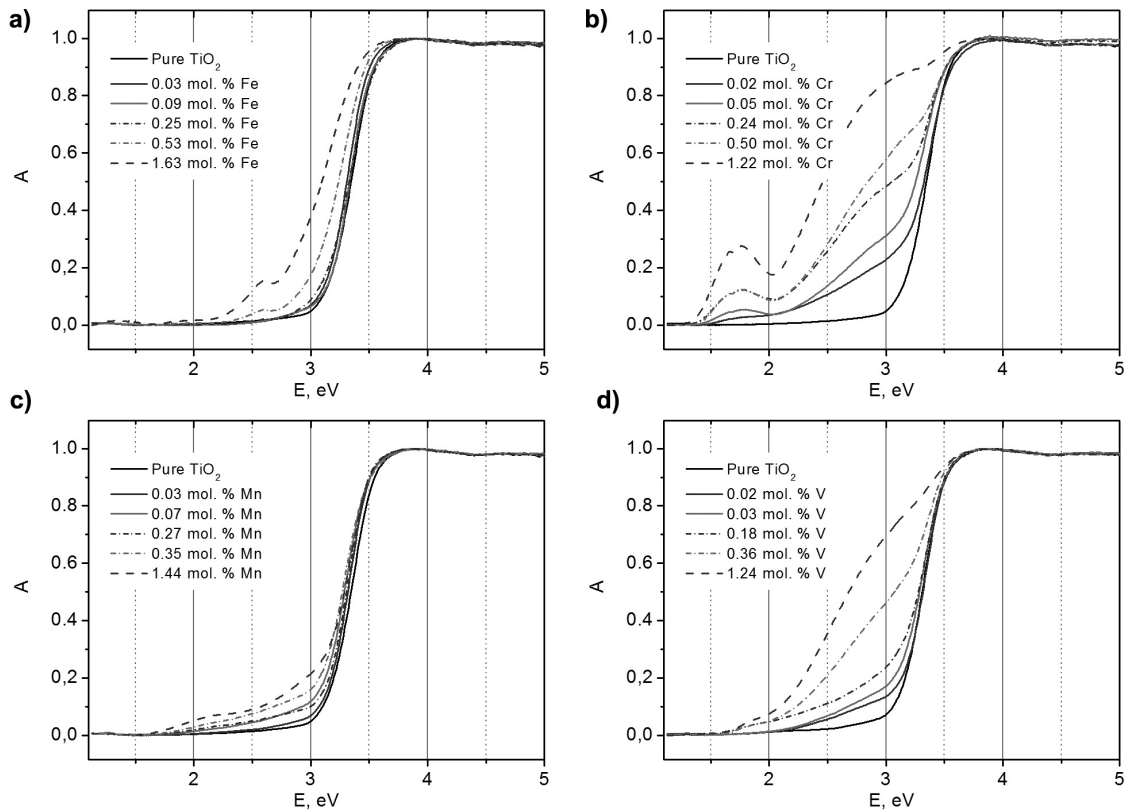


FIG. 2. UV-Vis spectra of nanocrystalline  $\text{TiO}_2$  and nanocrystalline  $\text{TiO}_2$  doped by Fe (a), Cr (b), Mn (c) and V (d) ions

case of V- and Cr- doped  $\text{TiO}_2$  the intensity of absorption which is associated with impurity is comparable with the intensity of  $\text{TiO}_2$  absorption edge.

It was mentioned before that all samples have similar nanocrystalline structure, coherent scattering region size and phase composition. The unit cell parameters for pure and doped samples also do not change significantly. Thus, one can assume that the physical band gap is also constant and the change of optical properties occurs due to the formation of new energy levels in the band gap. The value of the band gap and the positions of impurity-associated levels were determined by mathematical processing of UV-Vis spectra.

Anatase is the main component of the nanocrystalline TiO<sub>2</sub> sample according XRD data and it is an indirect semiconductor. The procedure of band gap determination for indirect semiconductors involves plotting of the absorption spectrum in coordinates  $\sqrt{\alpha}$  vs.  $h\nu$  and finding of the interceptions of the linear parts of the curve with the abscissa axis [27]. The values which are found by this approach correspond to phonon-assisted transitions. However there are no linear parts of the absorption curve in case of anatase (Fig. 3). Similar absorption spectrum was observed in anatase single crystals [31]. It was concluded that anatase absorption edge follows Urbach rule because the excitons are self-trapped. In case when the absorption edge is Urbach type, the absorption depends on photon energy as:

$$\alpha(E) = \alpha_0 \exp\left(-\sigma \frac{E_0 - E}{kT}\right),$$

where  $\alpha(E)$  is absorption coefficient,  $\sigma$  is the steepness parameter,  $E_0$  is optical gap value and  $E$  is photon energy. We estimated optical gap value  $E_0$  using this equation as the slope of the absorption curve in logarithmic coordinates and obtained the value of 3.35 eV which is in good agreement with the data provided in [28]. On the other hand there is significant discrepancy with the other literature data [29] where the band gap value of anatase was found to be only 3.05 eV. The authors of this work did not provide the details about the band gap calculation procedure and did not mention Urbach nature of anatase absorption edge.

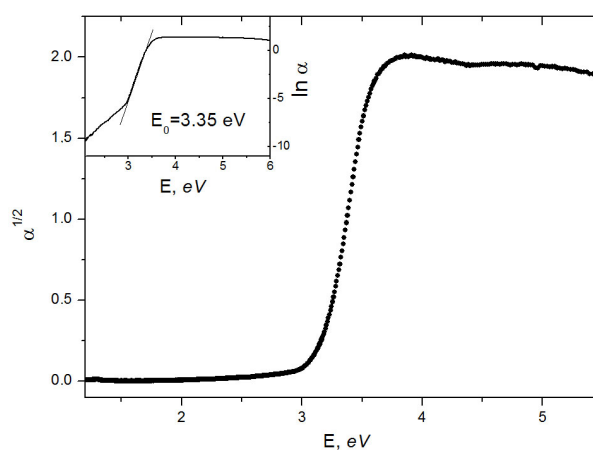
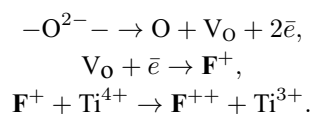


FIG. 3. UV-Vis spectrum of nanocrystalline TiO<sub>2</sub>  $\sqrt{\alpha}$  vs.  $h\nu$  and calculation of optical bang gap assuming Urbach tail (inset)

Further deconvolution of the spectra allowed us to determine the transition energies associated with defect levels in the band gap. The approach was suggested by Serpone, Kuznetsov, Rybchuk and Emeline for oxygen-deficient and nitrogen-doped titanium oxide [18–20,30]. In our work, the spectrum of undoped TiO<sub>2</sub> was subtracted from the spectra of doped samples and the residual spectrum was deconvoluted by Gaussian functions. The positions of maxima of Gaussian peaks were associated with different types of transitions. Some of these transitions are observed in all doped samples and there are the transitions which are characteristic for certain dopant. The deconvolution of the spectra of doped samples which Fig. 4. contain the highest concentrations of impurity are presented on Fig. 4 and the schematic representation of the transitions is presented on the Fig. 4.

Two bands, at approximately 2.7 eV and 2.9 eV, are present in the spectra of all doped samples. According to the data of Serpone and Emeline [18–20] they can be attributed to d-d transitions of Ti<sup>3+</sup> or may be associated with oxygen vacancy level in the band gap [31]. The formation of Ti<sup>3+</sup> ions in the lattice of TiO<sub>2</sub>, vacancies in anionic positions and color centers may occur due to partial reduction during decomposition of organic residuals during calcination:



The bands at 3.2 – 3.3 eV may be attributed to the transitions to exciton levels near the band gap edges.

All other bands differ in the spectra of the samples with different type of dopant and were associated with d-d transitions of impurity ions or with transitions from impurity level to  $E_c$ . The positions of impurity levels in nanocrystalline anatase TiO<sub>2</sub> were taken the same as experimental values for rutile single crystal [32]. The levels of Fe<sup>3+</sup>, Cr<sup>3+</sup>, V<sup>4+</sup> and Mn<sup>3+</sup> lie at 3.0, 2.7, 1.9 and 2.1 eV below  $E_c$  respectively.

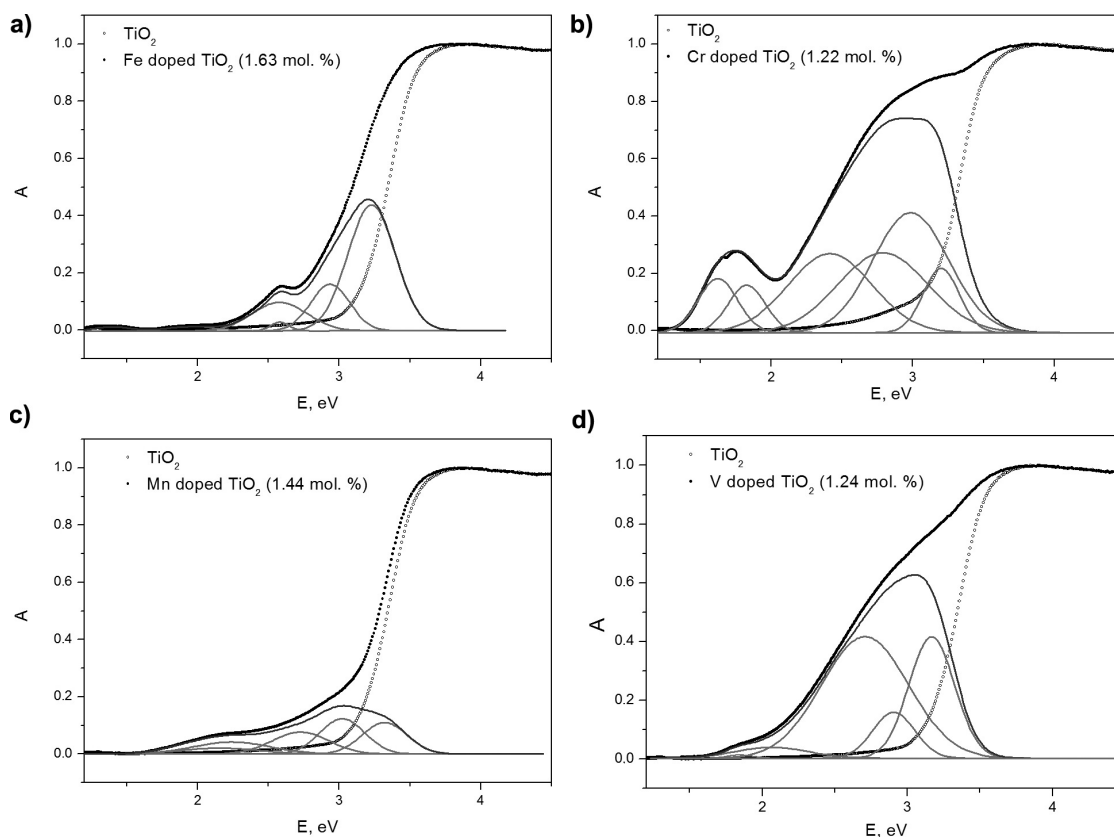


FIG. 4. Deconvolution of UV-Vis spectra of nanocrystalline  $\text{TiO}_2$  doped by Fe (a), Cr (b), Mn (c) and V (d) ions

In the case of Cr-doped  $\text{TiO}_2$ , we observe 3 bands with the energies 2.4, 1.8 and 1.6 eV. These energies are very close to the energies of d-d transitions of  $\text{Cr}^{3+}$  ions observed in Cr-doped spinel and ruby [33,34]. In both cases  $\text{Cr}^{3+}$  ion is in octahedral coordination and the crystal field of oxygen atoms which surround it may be assumed as similar. So, we conclude that these bands correspond to the d-d transitions of  $\text{Cr}^{3+}$  ions in anatase lattice.

The same approach can be used for interpreting the spectra of Fe-doped samples. The bands which are present in the spectra of Fe-doped samples at 1.4, 1.9 and 2.6 eV are very close to the bands of  $\text{Fe}^{3+}$  in spinel [35]. So, these bands correspond to d-d transitions of  $\text{Fe}^{3+}$  ions in anatase lattice.

The situation for V-doped and Mn-doped samples is different. The bands of d-d transitions of  $\text{Mn}^{3+}$  ion in spinel lattice and  $\text{V}^{4+}$  in garnet lattice in octahedral coordinations have energies of 2.9 and 2.4 eV respectively [36,37]. But according to the work of Mitsushima et al. the levels of  $\text{V}^{4+}$  and  $\text{Mn}^{3+}$  are sitting 2.1 and 1.9 eV below  $E_c$ . So, it is not possible to observe d-d transitions for these ions and the bands which are observed in the spectra of V- and Mn-doped samples can be attributed to the transition from the impurity level to  $E_c$ . The experimental values which have been observed in this work are 1.8 eV for V-doped anatase and 1.9 eV for Mn-doped anatase. The positions of the levels in the band gap of nanocrystalline  $\text{TiO}_2$  are provided on the Fig. 5.

The band at approximately 2.1 – 2.2 eV is also present in the spectra of all samples. It can be attributed to the transition associated with the color center:  $\text{F}^+ \rightarrow \text{F}^{+*}$  [18]. Sekiya et. al associates this band with  $\text{Ti}^{3+}$  d-d transition [31]. And Mitsushima attributes this transition to intrinsic defect states in  $\text{TiO}_2$  [32]. So this band may be assumed as one more defect-associated band in spectra of Mn- and V-doped samples.

The influence of doping on the photocatalytic properties of nanocrystalline  $\text{TiO}_2$  was studied in the reaction of methyl orange decoloration. The first order constants of the decoloration reaction for pure and doped samples are presented on the Fig. 6. We observe a significant decrease in the photocatalytic activity for all doped samples. Chromium and vanadium are the dopants which most effectively suppress photocatalytic activity.

Also, photocatalytic activity decreases in presence of Mn and Fe-impurities. Photocatalytic activity sharply drops in presence of very small impurity concentrations and then slightly increases in the Mn-doped series and

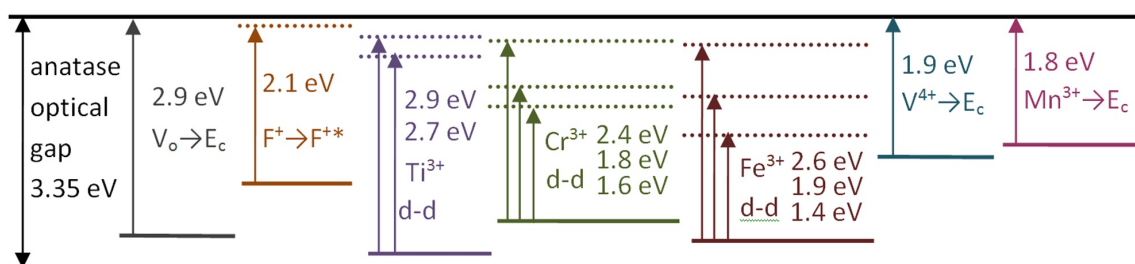


FIG. 5. The positions of energy levels in the band gap of nanocrystalline TiO<sub>2</sub> doped by ions of 3d-elements

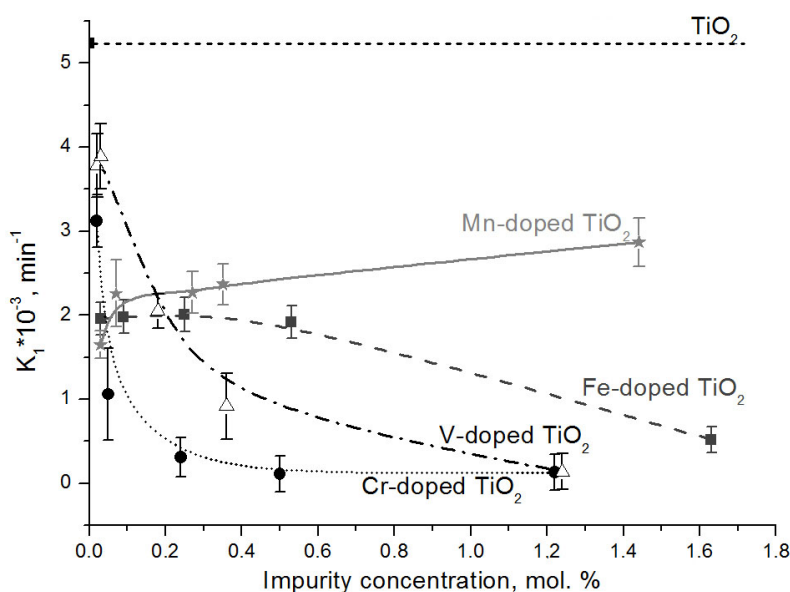


FIG. 6. First order reaction constants of the decoloration of methyl orange for nanocrystalline TiO<sub>2</sub> doped by ions of 3d-elements

decreases in the Fe-doped series. The absorption curves of Fe- and Mn- doped samples with low dopant concentrations are very close to the absorption curve of undoped sample. One can conclude that there may be the factors which influence photocatalytic activity in addition to the particle size, phase composition and optical properties.

So, if the structure and phase composition of doped by d-metal ions does not change in comparison with undoped samples, photocatalytic activity is effectively suppressed due to defect levels. Thus, doping by cations seems to be ineffective for developing materials with enhanced photocatalytic activity. Conversely, titanium oxide with small defect concentration is the most promising photocatalyst. The modification of its properties by preparing composites with metal particles and semiconductors indeed leads to the growth of photocatalytic activity [38,39].

On the other hand, the ability of 3d-metal ions to suppress photocatalytic activity may be also useful for some applications. For example, photocatalytic activity is not useful and even harmful in cosmetic pigments, paints, plastic fillers. In this case reactive oxygen species, which are generated due to photocatalytic reactions damage organic components of cosmetic, paint or plastic and doping by metal cations is effective way to prevent these adverse effects. Iron as non-toxic impurity may be used in TiO<sub>2</sub> cosmetic pigments to suppress their ability to generate reactive oxygen species under sunlight. Such pigments may provide a non-toxic alternative to known pigments like nanocrystalline cerium oxide doped by gadolinium [40].

#### 4. Conclusions

The influence of doping on photocatalytic activity and in association with optical properties without interference with the other factors was studied on the series of the samples of nanocrystalline TiO<sub>2</sub> doped by Cr, Fe, V and Mn with similar phase composition, surface area and coherent scattering region sizes. The impurities effectively suppress photocatalytic activity of TiO<sub>2</sub>. TiO<sub>2</sub>-based materials with suppressed photocatalytic activity can be used

as plastic fillers and cosmetic pigments because they will not generate active radicals under solar irradiation. UV-Vis spectral analysis of the samples allowed us to determine the nature of the levels, which are formed in the band gap. In case of all samples, we observe d-d transitions of  $Ti^{3+}$  ion and a transition from the color center to  $E_c$ . In case of Cr- and Fe-doped samples, we observe d-d transitions of these ions and in the spectra of Mn- and V-doped  $TiO_2$  the transitions from metal impurity level to  $E_c$  are present.

## Acknowledgements

This work was supported by Russian Science Foundation (research project 17-73-10493). The measurements on Rigaku D/MAX 2500 diffractometer and Zeiss Libra 200 electron microscope were have been done due to the Program of Development of M. V. Lomonosov State University.

## References

- [1] Herrmann J.-M. Detrimental cationic doping of titania in photocatalysis: why chromium  $Cr^{3+}$ -doping is a catastrophe for photocatalysis, both under UV- and visible irradiations. *New J. Chem.*, 2012, **36**, P. 883–890.
- [2] Bettinelli M., Speghini A., Falcomer D., Daldosso M., Dallacasa V., Romano V. Photocatalytic, spectroscopic and transport properties of lanthanide-doped  $TiO_2$  nanocrystals. *J. Phys.: Condens. Matter*, 2006, **18**, P. S2149–S2160.
- [3] Cui L., Wang Yu., Niu M., Chen G., Cheng Y. Synthesis and visible light photocatalysis of Fe-doped  $TiO_2$  mesoporous layers deposited on hollow glassmicrobeads. *Journal of Solid State Chemistry*, 2009, **182**, P. 2785–2790.
- [4] Karvinen S., Lamminmäk R.-J. Preparation and characterization of mesoporous visible-light-active anatase. *Solid State Sciences*, 2003, **5**, P. 1159–1166.
- [5] Kumbhar A., Chumanov G. Synthesis of iron(III)-doped titania nanoparticles and its application for photodegradation of sulforhodamine-B pollutant. *Journal of Nanoparticle Research*, 2005, **7**, P. 489–498.
- [6] Li G., Liu C., Liu Yu. Different effects of cerium ions doping on properties of anatase and rutile  $TiO_2$ . *Applied Surface Science*, 2006, **253**, P. 2481–2486.
- [7] Liu B., Wanga X., Caia G., Wen L., Song Y., Zhao X. Low temperature fabrication of V-doped  $TiO_2$  nanoparticles, structure and photocatalytic studies. *Journal of Hazardous Materials*, 2009, **169**, P. 1112–1118.
- [8] Liu S., Xie T., Chen Z., Wu J. Highly active V- $TiO_2$  for photocatalytic degradation of methyl orange. *Applied Surface Science*, 2009, **255**, P. 8587–8592.
- [9] Andreas Mattsson A., Leideborg M., Karin Larsson, Westin G., Osterlund L. Adsorption and Solar Light Decomposition of Acetone on Anatase  $TiO_2$  and Niobium Doped  $TiO_2$  Thin Films. *J. Phys. Chem. B*, 2006, **110**, P. 1210–1220.
- [10] Ranjit K.T., Willner I., Bossmann S.H., Braun A.M. Lanthanide Oxide Doped Titanium Dioxide Photocatalysts: Effective Photocatalysts for the Enhanced Degradation of Salicylic Acid and t-Cinnamic Acid. *Journal of Catalysis*, 2001, **204**(2), P. 305–313.
- [11] Xiao J., Peng T., Li R., Peng Z., Yan C. Preparation, phase transformation and photocatalytic activities of cerium-doped mesoporous titania nanoparticles. *Journal of Solid State Chemistry*, 2006, **179**, P. 1161–1170.
- [12] Xin B., Ren Z., Wang P., Liu J., Jing L., Fu H. Study on the mechanisms of photoinduced carriers separation and recombination for  $Fe^{3+}$ - $TiO_2$  photocatalysts. *Applied Surface Science*, 2007, **253**, P. 4390–4395.
- [13] Silva A.M.T., Silva C.G., Drazic G., Faria J.L. Ce-doped  $TiO_2$  for photocatalytic degradation of chlorophenol. *Catalysis Today*, 2009, **144**, P. 13–18.
- [14] Kemp T.J., McIntyre R.A., Transition metal-doped titanium(IV) dioxide: Characterisation and influence on photodegradation of poly(vinyl chloride). *Polymer Degradation and Stability*, 2006, **91**, P. 165–194.
- [15] Kolesnik I.V., Chebotaeva G.S., Yashina L.V., Konstantinova E.A., Eliseev A.A., Lukashin A.V., Tretyakov Yu.D. Preparation of nanocrystalline nitrogen-doped mesoporous titanium dioxide. *Mendeleev Communications*, 2012, **23**(1), P. 11–13.
- [16] Savio A.K.P.D., Fletcher J., Robles Hernandez F.C. Sonosynthesis of nanostructured  $TiO_2$  doped with transition metals having variable bandgap. *Ceramics International*, 2013, **39**, P. 2753–2765.
- [17] Di Paola A., Marci G., Palmisano L., Schiavello M., Uosaki K., Ikeda S., B. Ohtani B. Preparation of Polycrystalline  $TiO_2$  Photocatalysts Impregnated with Various Transition Metal Ions: Characterization and Photocatalytic Activity for the Degradation of 4-Nitrophenol. *J. Phys. Chem. B*, 2002, **106**, P. 637–645.
- [18] Serpone N. Is the Band Gap of Pristine  $TiO_2$  Narrowed by Anion- and Cation-Doping of Titanium Dioxide in Second-Generation Photocatalysts? *J. Phys. Chem. B*, 2006, **110**, P. 24287–24293.
- [19] Kuznetsov V.N., Serpone N. Visible Light Absorption by Various Titanium Dioxide Specimens. *J. Phys. Chem. B*, 2006, **110**, P. 25203–25209.
- [20] Kuznetsov V.N., Serpone N. On the Origin of the Spectral Bands in the Visible Absorption Spectra of Visible-Light-Active  $TiO_2$  Specimens Analysis and Assignments. *J. Phys. Chem. C*, 2009, **113**, P. 15110–15123.
- [21] Lebedev V.A., Kozlov D.A., Kolesnik I.V., Poluboyarinov A.S., Becerikli A.E. Grnert W., Garshev A.V. The amorphous phase in titania and its influence on photocatalytic properties. *Applied Catalysis B: Environmental*, 2016, **195**, P. 39–47.
- [22] Di Paola A., Bellardita M., Palmisano L., Barbierikova Z., Brezova V. Influence of crystallinity and OH surface density on the photocatalytic activity of  $TiO_2$  powders. *Journal of Photochemistry and Photobiology A: Chemistry*, 2013, **273**, P. 59–67.
- [23] Sakatani Y., Grosso D., Nicole L., Boissiere C., Soler-Illia G.J. de A.A., Sanchez C.J. Optimised photocatalytic activity of grid-like mesoporous  $TiO_2$  films: effect of crystallinity, pore size distribution, and pore accessibility. *Mater. Chem.*, 2006, **16**, P. 77–82.
- [24] Petricek X.V., Dusek M., Palatinus L. Crystallographic Computing System JANA2006: General features. *Zeitschrift für Kristallographie - Crystalline Materials*, 2014, **229**, P. 345352–34356.
- [25] Almjasheva O.V. Formation and structural transformations of nanoparticles in the  $TiO_2$ - $H_2O$  system. *Nanosystems: physics, chemistry, mathematics*, 2016, **7**(6), P. 1031–1049.

- [26] Vildanova M.F., Kozlov S.S., Nikolskaia A.B., Shevaleevskiy O.I., Tsvetkov N.A., Alexeeva O.V., Larina L.L. Niobium-doped titanium dioxide nanoparticles for electron transport layers in perovskite solar cells. *Nanosystems: physics, chemistry, mathematics*, 2017, **8**(4), P. 540–545.
- [27] Pankove J.I. *Optical Processes in Semiconductors*. Dover Publications, Inc., New York, 1975, 343 p.
- [28] Tang H., Levy F., Berger H., Schmid P.E. Urbach tail of anatase TiO<sub>2</sub>. *Physical Review B*, 1995, **52**(11), P. 7771–7774.
- [29] Di Paola A., Bellardita M., Palmisano L., Parrino F. Junction Effect on the Photocatalytic Activity of Mixed-Phase TiO<sub>2</sub> Nanoparticles. *ECS Transactions*, 2010, **25**(42), P. 29-35.
- [30] Emeline A.V., Kuznetsov V.N., Rybchuk V.K., Serpone N. Visible-Light-Active Titania Photocatalysts: The Case of N-Doped TiO<sub>2</sub> - Properties and Some Fundamental Issues. *International Journal of Photoenergy*, 2008, P. 1-19.
- [31] Sekiya T., Ichimura K., Igarashi M., Kurita S. Absorption spectra of anatase TiO<sub>2</sub> single crystals heat-treated under oxygen atmosphere. *Journal of Physics and Chemistry of Solids*, 2000, **61**, P. 1237–1242.
- [32] Mizushima K., Tanaka M., Asai A., Iida S., Goodenough J.B. Impurity Levels Of Iron-Group Ions In TiO<sub>2</sub>. *J Phys. Chem. Solids*, 1979, **10**, P. 1129–1140
- [33] Wood D.L., Imbusch G.F., Macfarlane R.M., Kisliuk P., and Larkin D.M. Optical Spectrum of Cr<sup>3+</sup> Ions in Spinels. *The Journal of Chemical Physics*, 1968, **48**, P. 5255–5263.
- [34] Low W. Absorption Lines of Cr<sup>3+</sup> in Ruby. *The Journal of Chemical Physics*, 1960, **33**, P. 1162–1163.
- [35] Reddy B.J., Frost R.L. Spectroscopic characterization of chromite from the Moa-Baracoa Ophiolitic Massif, Cuba. *Spectrochimica Acta Part A*, 2005, **61**, P. 1721–1728.
- [36] Bosi F., Hälenius U., Andreozzi G.B., Skogby H., Lucchesin S. Structural refinement and crystal chemistry of Mn-doped spinel: A case for tetrahedrally coordinated Mn<sup>3+</sup> in an oxygen-based structure. *American Mineralogist*, 2007, **92**, P. 27–33.
- [37] Brenier A., Madej C., Pedrini C., Boulon G. Crystal growth and luminescence properties of calcium- and vanadium-doped gadolinium gallium garnet. *Chemical Physics Letters*, 1991, **177**(6), P. 590–592.
- [38] Karthikeyan N., Narayanan V., Stephen A. Visible light degradation of textile effluent using nanostructured TiO<sub>2</sub>/Ag/CuO photocatalysts. *Nanosystems: Physics, Chemistry, Mathematics*, 2016, **7**(4), P. 695–698.
- [39] Kozlov D.A., Lebedev V.A., Polyakov A.Yu, Khazova K.M., Garshev A.V. The microstructure effect on the Au/TiO<sub>2</sub> and Ag/TiO<sub>2</sub> nanocomposites photocatalytic activity. *Nanosystems: Physics, Chemistry, Mathematics*, 2018, **9**(2), P. 266–278.
- [40] Popov A.L., Savintseva I.V., Mysina E.A., Shcherbakov A.B., Popova N.R., Ivanova O.S., Ivanov V.K. Cytotoxicity analysis of gadolinium doped cerium oxide nanoparticles on human mesenchymal stem cells. *Nanosystems: Physics, Chemistry, Mathematics*, 2018, **9**(3), P. 18–25.